Hexagonally Patterned Lamellar Morphology in ABC Triblock Copolymer/Aluminosilicate Nanocomposites

Gilman E. S. Toombes,[†,‡,§] Surbhi Mahajan,[‡,§,||] Malcolm Thomas,[⊥] Phong Du,[‡,||] Mark W. Tate,[†] Sol M. Gruner,[†,#] and Ulrich Wiesner*[,||]

Department of Physics, Department of Materials Science and Engineering, Cornell Center for Materials Research, and Cornell High Energy Synchrotron Source (CHESS), Cornell University, Ithaca, New York 14853

Received October 2, 2007. Revised Manuscript Received February 13, 2008

X-ray scattering and electron microscopy were used to characterize the structure of poly(ethylene-*alt*-propylene-*block*-ethylene oxide-*block*-*n*-hexyl methacrylate) (PEP-*b*-PEO-*b*-PHMA) triblock copolymer/aluminosilicate hybrid materials in which the volume fraction of the PEP end-block ($0.09 \leq f_{PEP} \leq 0.12$) was much smaller than that of the PEO-aluminosilicate ($0.28 \leq f_{PEO+aluminosilicate} \leq 0.44$) and PHMA ($0.47 \leq f_{PHMA} \leq 0.60$) domains. These hybrid compounds formed a hexagonally patterned lamellar morphology in which the lamellae were aligned parallel to the material surface (lamellar repeat spacing $= 33.0 \pm 3.3$ nm, in-plane row spacing $= 21.7 \pm 1.9$ nm). Both the PHMA and PEO-aluminosilicate phases formed continuous, two-dimensional domains permitting individual sheets of the material to be isolated by dispersal in organic solvent. Within each sheet, the lamellar PEO-aluminosilicate domain was hexagonally patterned by an array of "holes" with lower aluminosilicate density. Since the enthalpy of mixing for the small PEP end-block and PEO-aluminosilicate phase is very large, the "holes" in the PEO-aluminosilicate sheet may correspond to micellar PEP domains forming either dimples in the surface of the sheet or pillars spanning the sheet as in the proposed "pillared-lamellae" morphology (*Macromolecules* **2001**, *34*, 6994−7008). These results suggest that the use of ABC copolymers as structure-directing agents may provide access to a wide range of morphologies.

Introduction

Microphase separation in block copolymers can be used to direct the assembly of inorganic precursors into nanometer-scale structures.[1–3] These block copolymer/inorganic materials are of interest for applications such as porous electrodes, membranes, catalysts, low dielectric insulators and photonic band gap materials.[4,5] Using block copolymers with two-domain AB or ABA architectures, structures with lamellar, hexagonal and cubic symmetry have been formed in silica-type materials.[6–8] However, only a limited number of morphologies are accessible with AB or ABA block copolymers, especially in comparison to the many structures found in ABC triblock copolymers.[9–11] The use of ABC triblock copolymers as structure-directing agents may provide access to noncentrosymmetric,[12] chiral[13] and several network structures[14,15] and could allow the independent structuring of two or three types of inorganic precursor.[2,16] Despite this potential, harnessing the complex phase behavior of ABC triblock copolymers remains challenging.[17]

This report describes a hexagonally patterned lamellar ABC triblock copolymer/aluminosilicate structure formed with the amphiphilic poly(ethylene-*alt*-propylene-*block*-ethylene oxide-*block*-*n*-hexyl methacrylate) (PEP-*b*-PEO-*b*-

* Corresponding author. E-mail: ubw1@cornell.edu.
† Department of Physics.
‡ Present addresses: PCC UMR 168, Institut Curie, Paris, 11 rue Pierre et Marie Curie, Paris 75005, France (G.E.S.T.). DuPont Central Research and Development, Experimental Station, Route 141 and Henry Clay, Wilmington, DE 19880-0328 (S.M., P.D.).
§ These authors contributed equally to this work.
|| Department of Materials Science and Engineering.
⊥ Cornell Center for Materials Research.
Cornell High Energy Synchrotron Source.

(1) Thompson, R. B.; Ginzburg, V. V.; Matsen, M. W.; Balazs, A. C. *Science (Washington, D.C.)* **2001**, *292*, 2469–2472.
(2) Bockstaller, M. R.; Mickiewicz, R. A.; Thomas, E. L. *Adv. Mater. (Weinheim, Ger.)* **2005**, *17*, 1331–1349.
(3) Shenhar, R.; Norsten, T. B.; Rotello, V. M. *Adv. Mater. (Weinheim, Ger.)* **2005**, *17*, 657–669.
(4) Kresge, C. T.; Leonowicz, M. E.; Roth, W. J.; Vartuli, J. C.; Beck, J. S. *Nature (London)* **1992**, *359*, 710–712.
(5) Soler-Illia, G. J. D.; Sanchez, C.; Lebeau, B.; Patarin, J. *Chem. Rev.* **2002**, *102*, 4093–4138.
(6) Bagshaw, S. A.; Prouzet, E.; Pinnavaia, T. J. *Science (Washington, D.C.)* **1995**, *269*, 1242–1244.
(7) Templin, M.; Franck, A.; Du Chesene, A.; Leist, H.; Zhang, Y.; Ulrich, R.; Schadler, V.; Wiesner, U. *Science (Washington, D.C.)* **1997**, *278*, 1795–1798.
(8) Zhao, D. Y.; Feng, J. L.; Huo, Q. S.; Melosh, N.; Fredrickson, G. H.; Chmelka, B. F.; Stucky, G. D. *Science (Washington, D.C.)* **1998**, *279*, 548–552.
(9) Matsushita, Y.; Choshi, H.; Fujimoto, T.; Nagasawa, M. *Macromolecules* **1980**, *13*, 1053–1058.
(10) Zheng, W.; Wang, Z. G. *Macromolecules* **1995**, *28*, 7215–7223.
(11) Bates, F. S.; Fredrickson, G. H. *Phys. Today* **1999**, *52* (February), 32–38.
(12) Goldacker, T.; Abetz, V.; Stadler, R.; Erukhimovich, I.; Leibler, L. *Nature (London)* **1999**, *398*, 137–139.
(13) Krappe, U.; Stadler, R.; Voigt-Martin, I. *Macromolecules* **1995**, *28*, 4558–4561.
(14) Mogi, Y.; Kotsuji, H.; Kaneko, Y.; Mori, K.; Matsushita, Y.; Noda, I. *Macromolecules* **1992**, *25*, 5412–5415.
(15) Epps, T. H.; Cochran, E. W.; Bailey, T. S.; Waletzko, R. S.; Hardy, C. M.; Bates, F. S. *Macromolecules* **2004**, *37*, 7085–7088.
(16) Chiu, J. J.; Kim, B. J.; Kramer, E. J.; Pine, D. J. *J. Am. Chem. Soc.* **2005**, *127*, 5036–5037.
(17) Ludwigs, S.; Boker, A.; Voronov, A. J.; Rehse, N.; Magerle, R.; Krausch, G. *Nat. Mater.* **2003**, *2*, 744–747.

10.1021/cm702842b CCC: $40.75
Published on Web 04/23/2008

Table 1. Composition of ABC Copolymer/Aluminosilicate Compounds[a]

compound	f_{PEP}	$f_{PEO+aluminosilicate}$	f_{PHMA}
H28	0.12	0.28	0.60
H34	0.11	0.34	0.55
H39	0.10	0.39	0.51
H44	0.09	0.44	0.47

[a] Domain volume fractions were calculated assuming room temperature densities of $\rho_{PEP} = 0.855$ g/cm^3,[23] $\rho_{PEO+aluminosilicate} = 1.4$ g/cm^3,[19] and $\rho_{PHMA} = 1.007$ g/cm^3.[25]

PHMA) copolymer[18] mixed with aluminosilicate precursors. For this polymer, the Flory−Huggins interactions parameters ($\chi_{PEP/PEO}N \approx 350$, $\chi_{PEO/PHMA}N \approx 130$, $\chi_{PEP/PHMA}N \approx 50$) favor optional contact between PEP and PHMA domains over the obligatory PEP/PEO and PEO/PHMA interfaces. The aluminosilicate partitions into the hydrophilic PEO block.[7,19] Table 1 summarizes the block volume fractions of the hybrid compounds. The volume fraction of the PEP block ($0.09 \leq f_{PEP} \leq 0.12$) was much smaller than the PEO-aluminosilicate ($0.28 \leq f_{PEO+Aluminosilicate} \leq 0.44$) and PHMA ($0.47 \leq f_{PHMA} \leq 0.60$) domains.

The composition of these hybrid compounds ($f_A \ll f_B, f_C$) corresponds to the small end-block regime[20] of interest for studying the transition from two-domain diblock to three-domain triblock morphologies. In a diblock PEO-*b*-PHMA copolymer/aluminosilicate material,[21] the PHMA and PEO-aluminosilicate phases can form a simple lamellar morphology as illustrated in Figure 1a. However, in the triblock copolymer, the enthalpic cost for the PEP block mixing in the PEO-aluminosilicate domain is very large. These unfavorable interactions can be reduced by the formation of micellar PEP domains as in the "balls-in-lamellae"[10] (Figure 1b), "cylinders-in-lamellae",[22] dimple (Figure 1c) and "pillared-lamellae"[20] (Figure 1d−f) structures.

For these hybrid materials, small angle X-ray scattering (SAXS) and electron microscopy data indicate both the PHMA and PEO-aluminosilicate phases formed lamellar sheets aligned parallel to the surface of the film. Scanning transmission electron microsopy (STEM) images of individual layers of the material showed a hexagonal mesh structure within each PEO-aluminosilicate layer, suggesting the PEP block formed round, micellar domains. These results confirm that ABC block copolymers can be used to direct silica-type materials into complex ABC block copolymer morphologies.

Experimental Methods

Materials Synthesis. Poly(ethylene-*alt*-propylene-*block*-ethylene oxide-*block*-*n*-hexyl methacrylate) (PEP-*b*-PEO-*b*-PHMA) was synthesized via stepwise anionic polymerization, catalytic hydrogenation and atom transfer radical polymerization as described earlier.[18] The molecular weight ($M_n = 48520$ g/mol) and polydispersity ($M_w/M_n = 1.13$) were determined via NMR and GPC. Block volume fractions were $f_{PEP} = 0.15$, $f_{PEO} = 0.11$ and $f_{PHMA} = 0.74$, assuming the block densities correspond to the room temperature densities of the homopolymers.[23−25] The Flory−Huggins interaction parameters for the three blocks were approximately $\chi_{PEP/PEO}N = 350$, $\chi_{PEO/PHMA}N = 130$, and $\chi_{PEP/PHMA}N = 50$ as estimated using the approximation of Hildebrand and Scott,[26]

$$\chi_{ij} = \frac{V_{ref}(\delta_i - \delta_j)^2}{RT}$$

where V_{ref} is the segment reference volume and δ_i the Hildebrand solubility parameter for polymer i (δ_{PEP}[27] $= 16.0$ (MPa)$^{1/2}$, δ_{PEO}[28] $= 20.2$ (MPa)$^{1/2}$, and δ_{PHMA}[28] $= 17.6$ (MPa)$^{1/2}$).

ABC copolymer-aluminosilicate composites were prepared following a general procedure described previously.[7,19] Briefly, the

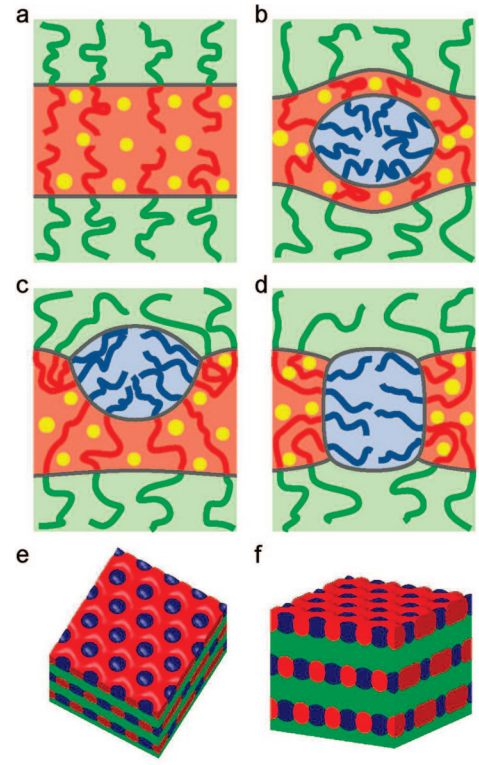

Figure 1. Structural models for PEP-*b*-PEO-*b*-PHMA block copolymer/aluminosilicate lamellar morphologies with a small PEP block. In the absence of the PEP block, the PEO (red) and PHMA (green) chains stretch into their respective domains while the aluminosilicate particles (yellow) partition into the hydrophilic PEO domain (a). Possible domain structures discussed in the text are illustrated as follows: In the "balls-in-lamellae" structure the small PEP block (blue) forms round micellar domains (b). Dimple structure with PEP micelles at the PHMA/PEO-aluminosilicate interface (c). In the "pillared-lamellae" structure the PEP domain form pillars spanning across the PEO-aluminosilicate domain (d). Top (e) and side (f) views of the "pillared-lamellae" structure. (n.b. In an ABC copolymer, the curvature of AC domain interfaces depends on a number of considerations and the shape of PEP domains shown are only approximate.)

(18) Mahajan, S.; Cho, B. K.; Allgaier, A.; Fetters, L. J.; Coates, G. W.; Wiesner, U. *Macromol. Rapid Commun.* **2004**, *25*, 1889–1894.
(19) Jain, A.; Wiesner, U. *Macromolecules* **2004**, *37*, 5665–5670.
(20) Bailey, T. S.; Pham, H. D.; Bates, F. *Macromolecules* **2001**, *34*, 6994–7008.
(21) Renker, S.; Mahajan, S.; Babski, D. T.; Schnell, I.; Jain, A.; Gutmann, J.; Zhang, Y.; Gruner, S. M.; Spiess, H. W.; Wiesner, U. *Macromol. Chem. Phys.* **2004**, *205*, 1021–1030.
(22) Ludwigs, S.; Boker, A.; Abetz, V.; Muller, A. H. E.; Krausch, G. *Polymer* **2003**, *44*, 6815–6823.
(23) Fetters, L. J.; Lohse, D. J.; Richter, D.; Witten, T. A.; Zirkel, A. *Macromolecules* **1994**, *27*, 4639–4647.
(24) Zhu, L.; Cheng, S. Z. D.; Calhoun, B. H.; Ge, Q.; Quirk, R. P.; Thomas, E. L.; Hsiao, B. S.; Yeh, F.; Lotz, B. *Polymer* **2001**, *42*, 5829–5839.
(25) Rogers, S. S.; Mandelkern, L. *J. Phys. Chem.* **1957**, *61* (7), 985–991.
(26) Madkour, T. M. *Chem. Phys.* **2001**, *274*, 187–198.
(27) Schmidt, S. C.; Hillmyer, M. A. *J. Polym. Sci. B* **2002**, *40*, 2364–2376.
(28) Brandrup, J.; Immergut, E. H. *Polymer Handbook*, 3rd ed.; J. Wiley & Sons: New York, 1989; Chapter VII, pp 554−555.

ABC copolymer was dissolved in a 50−50 mixture of tetrahydrofuran and chloroform to form a 2% solution by weight. In a second vial, a sol of 3-(glycidyloxypropyl) trimethoxysilane (GLYMO) and aluminum *sec*-butoxide (mole ratio of 8:2) was prepared following a two-step acid catalyzed hydrolysis procedure described previously.[7] For each hybrid material, appropriate volumes of the copolymer solution and this sol were combined and the resulting solution stirred for one hour. This solution was then transferred to glass evaporation dishes and films of the copolymer/aluminosilicate material were cast by evaporation of solvents and byproducts on a hot-plate at 50 °C. The resulting clear films (∼1 mm thick) were then annealed for 1 h at 130 °C in a vacuum oven to remove residual solvent. For each film, volume fractions for the PEO-aluminosilicate domain ($f_{PEO+aluminosilicate}$) were calculated assuming a density of 1.4 g/cm^3 for the PEO-aluminosilicate phase;[19] compositions are reported in Table 1.

X-ray Scattering. Small and wide-angle X-ray scattering data were gathered using a laboratory source. Briefly, Cu K_α X-rays (λ = 0.154nm) were generated with a Rigaku RU-3HR generator (voltage = 42 kV, current = 56mA, 2 mm × 0.2 mm point focus on the copper anode), filtered by a nickel foil (thickness = 10 μm; Goodfellow, PA) and focused and further monochromatized with a pair of Franks mirrors.[29] The flux at the sample was ∼4 × 10^7 X-ray photons per second in a ∼1 mm × 1 mm beam. Small angle X-ray scattering (SAXS) data was gathered using 60 cm or 100 cm flight tubes while wide angle X-ray scattering (WAXS) was measured using a 1.5 cm flight tube. A small circle of lead tape (typical diameter of 2−3 mm) at the end of the flight tube blocked the transmitted X-ray beam while the scattered X-rays were imaged with a home-built 2-D X-ray area detector.[30] The distance from the sample to detector and position of the beam center were determined using silver behenate ($d_{lamellar}$ = 5.8376 nm)[31] and silver stearate ($d_{lamellar}$ = 4.868 nm)[32] calibrants. In the text, scattering lengths are given as $s = 2\sin(\theta)/\lambda$, where 2θ is the total scattering angle and the quoted uncertainty represents the half-width at half maximum (HWHM) of the scattering peak.

Samples of the hybrid material were cut to size (1 mm wide × 5 mm long) and positioned using a mechanical rotation stage. To study the effect of solvent on the hybrid material, samples were placed in a standard glass X-ray capillary (d = 1.5 mm, Charles Supper, MA) and a small amount (5−15 μL) of cyclohexane added. The capillary was sealed with Parafilm M (Alcan Packaging, WI) to slow the escape of the solvent, and SAXS data gathered as the solvent slowly evaporated.

Oriented samples of the parent ABC block copolymer were prepared using a small, home-built shear cell. Specimens (∼7 mm long × 4 mm wide × 1.5 mm deep) were pressed into the shear cell. Under rough vacuum, the sample was heated to 75 °C and then sheared (∼150% shear at ∼0.5 Hz) for 5 min. The shear cell was then cooled back to room temperature (∼1 °C/minute) and the polymer removed and studied via SAXS. Solvent annealed samples of the parent ABC copolymer were prepared by heating the copolymer to T = 100 °C before exposing it to a cyclohexane vapor (∼50 kPa pressure). After 30 min annealing in the cyclohexane vapor, the sample was dried out using a rough vacuum (2 h) before cooling the sample back to room temperature (∼1 °C/min).

Microscopy. Cross-sections of the hybrid materials were prepared by freeze-fracture. Small (6 mm × 2 mm × 1 mm) samples of the hybrid material were held with tweezers and frozen by dipping into liquid nitrogen. While under the liquid nitrogen, the end of the sample was snapped off to expose a fresh cross-section perpendicular to the surface of the film. After thawing, samples were imaged at room temperature with a LEO 1550 field emission scanning electron microscope (FE-SEM) using the secondary electron signal and an accelerating voltage of 2 kV. For transmission electron microscopy (TEM), thin sections (50−100 nm thick) of the hybrid material were cut using a Leica Ultracut UCT microtome at 210 K and transferred to copper mesh TEM grid with a thin carbon layer. Bright-field TEM was performed using a JEOL 1200EX microscope operating at 120 kV.

Individual layers of the hybrid material were isolated by dispersing the hybrid material in an organic solvent (1 mg hybrid/1 g of toluene) for 12 h followed by mild sonication of the resulting solution.[33] Single drops of this solution were then placed onto a copper mesh TEM grid with a thin carbon layer and the solvent was allowed to evaporate. High resolution annular dark-field imaging and parallel electron energy loss spectroscopy (PEELS) of these samples were performed using the Cornell VG-HB501UX 100 keV UHV-STEM.[34] Additional STEM was performed using a LEO 1550 FE-SEM microscope fitted with a 4-quadrant solid-state STEM detector (accelerating voltage 30 kV). The individual sheets were also examined via Atomic Force Microscopy (AFM) by drop-coating the dispersed solution onto a silicon substrate (1 cm × 1 cm) and allowing the solvent to evaporate. The samples were imaged using a Veeco Nanoscope III Multimode scanning probe microscope employing tapping mode etched silicon tips.

Structural Models. The hybrid material structure was modeled in MATLAB using level set functions[35] consistent with block volume fractions and unit cell dimensions determined from SAXS, AFM, and STEM data. Fourier coefficients of the structural models were evaluated numerically and compared to the measured SAXS structure factors.

Results

All four compounds (Table 1) shared a common morphology of hexagonally patterned aluminosilicate sheets aligned parallel to the film surface (Figure 1e,f). For clarity, structural data for compound **H34** is used to summarize the common features of the morphology before then considering small variations in structure between the four compounds.

SAXS. Figure 2 shows 2-dimensional SAXS from compound **H34** in which the sample was oriented so that the normal to the film surface was directed along the *y*-axis (vertical) of the SAXS pattern. For this orientation, scattering along the *y*-axis (vertical) reflects order along the direction of the film normal while structure within the plane of the film leads to scattering along the *x*-axis (horizontal). The scattering pattern did not change when the sample was rotated about the film normal (*y*-axis), indicating simple fiber-type alignment of the structure with respect to the film surface.[36] The position and intensity of scattering along the horizontal layer and vertical row lines is summarized in Table 2.

(29) Hajduk, D. A. Ph.D. Thesis, Princeton University, 1994; pp 45−54.
(30) Tate, M. W.; Eikenberry, E. F.; Barna, S. L.; Wall, M. E.; Lowrance, J. L.; Gruner, S. M. *J. Appl. Crystallogr.* **1995**, *28*, 196–205.
(31) Blanton, T. N.; Huang, T. C.; Toraya, H.; Hubbard, C. R.; Robie, S. B.; Louër, D.; Göbel, H. E.; Will, G.; Gilles, R.; Raftery, T. *Powder Diffr.* **1995**, *10* (2), 91–95.
(32) Vand, V.; Aitken, A.; Campbell, R. K. *Acta Crystallogr.* **1949**, *2*, 398–403.
(33) Ulrich, R.; Du Chesne, A.; Templin, M.; Wiesner, U. *Adv. Mater. (Weinheim, Ger.)* **1999**, *11*, 141–146.
(34) Muller, D. A.; Singh, D. J.; Silcox, J. *Phys. Rev. B* **1998**, *57*, 8181–8202.
(35) Wohlgemuth, M.; Yufa, N.; Hoffman, J.; Thomas, E. *Macromolecules* **2001**, *34*, 6083–6089.
(36) Finkenstadt, V. L.; Millane, R. P. *Acta Crystallogr., Sect. A* **1998**, *54*, 240–248.

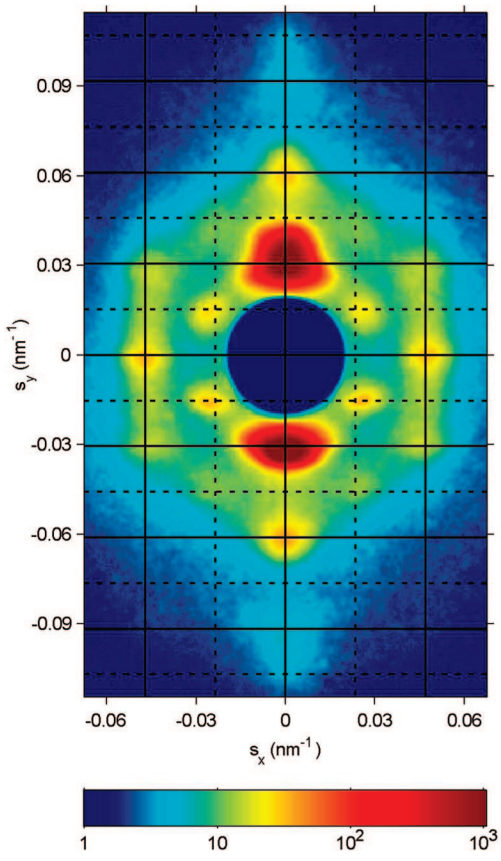

Figure 2. 2-D SAXS (logarithmic scale) from compound **H34** with the sample's surface normal directed along the vertical axis. The solid layer (horizontal) and row (vertical) lines mark repeat spacings of $d_l = 33.0 \pm 3.3$ nm ($\Delta s_y = 0.030 \pm 0.003$ nm^{-1}) and $d_r = 21.7 \pm 1.9$ nm ($\Delta s_x = 0.046 \pm 0.004$ nm^{-1}) respectively as reported in Table 2. Dotted layer and row lines correspond to a doubled unit cell.

Several features of the structure can be clearly resolved in the SAXS pattern. First, the three orders of Bragg spots along the vertical axis ($\Delta s_y = 0.030 \pm 0.003$ nm^{-1}) correspond to the lamellar stacking ($d_l = 33.0 \pm 3.3$ nm) of aluminosilicate sheets oriented parallel to the film surface. The narrow angular width of these spots (FWHM = 11°) confirms the lamellae are strongly aligned during the solvent-casting process.[37,38] Second, the intense, in-plane scattering along the vertical row lines at $|s_x| = 0.046 \pm 0.004$ nm^{-1} indicates periodic structure within the sheets with a repeat spacing of $d_r = 21.7 \pm 1.9$ nm. The integrated scattering intensity along these row lines is quite strong (~75% of the intensity of the first lamellar peak).

This strong scattering reflects the presence of large in-plane modulations of the PEO-aluminosilicate density, as is evident from structure factors calculated for the pillared-lamellae model shown in Figure 1e,f. In this structure the cylindrical PEP domains ($f_{PEP} = 0.11$) form pillars running through each PEO-aluminosilicate sheet ($f_{PEO+aluminosilicate} = 0.34$) in a 2-layer ABAB type stacking. Assuming room temperature densities for the PEP, PHMA and PEO+aluminosilicate domains, the outer row lines ($|s_x| = 0.046 \pm 0.004$ nm^{-1}) have an integrated intensity of 90% to 110% of the intensity of the first order lamellar Bragg peaks ($s_x = 0$ nm^{-1}, $|s_y| = 0.030 \pm 0.003$ nm^{-1}). Thus, the observed intensity for the outer row lines is largely consistent with the intensity expected for a pillared lamellae structure.

However, in the actual material the sheets cannot be stacked with long-range, periodic order or the scattering along the row lines would form Bragg Spots rather than the observed Bragg Rods. Such stacking disorder is frequently observed in hexagonal layered structures when the two-layer (ABABA) and three-layer (ABCABCA...) stackings are nearly degenerate.[39,40] Finally, as discussed in later sections, a unit cell doubling is suggested by the inner Bragg spots marked by the dotted row and layer lines ($|s_x| = 0.025 \pm 0.003$ nm^{-1}, $|s_y| = 0.014 \pm 0.003$ nm^{-1}).

The response of the hybrid materials to changes in temperature and solvent content provide further support for this interpretation of the SAXS data. A lamellar block copolymer/aluminosilicate material should preferentially deform along its lamellar axis because the covalent bonding network within each PEO-aluminosilicate layer constrains in-plane deformations. Because the middle PEO block of each chain is embedded within the covalent aluminosilicate network, shape changes in the sample should be directly reflected in the unit cell dimensions. Thus, following thermal expansion or swelling due to solvent uptake, the layer lines (lamellar ordering) should shift while the row lines (in-plane ordering) should remain fixed.

Figure 3a shows the change in lamellar and in-plane cell dimensions as a function of temperature. The linear thermal expansion coefficient ($4.33 \pm 0.11 \times 10^{-4}$ K^{-1}) along the lamellar direction was 7.5 ± 1 times the expansion coefficient in the in-plane direction ($5.8 \pm 0.8 \times 10^{-5}$ K^{-1}), confirming the anisotropic thermal expansion of the structure along the lamellar axis. Similarly, when **H34** was exposed to a nonpolar solvent (cyclohexane) the structure within the sheets remained essentially unchanged ($d_r = 21.7 \pm 1.9$ nm) while the adjoining PHMA domains swelled, as illustrated by the 50 ± 3% increase in lamellar spacing shown in Figure 3b. Remarkably, following evaporation of the solvent, the structure relaxed to the initial state as shown in Figure 3c (compare to Figure 2). The extreme anisotropy of the hybrid materials provides strong support for a hexagonally patterned lamellar structure.

Microscopy. Real-space images of the hybrid material were obtained from the bulk material, thin sections, and individual sheets isolated by solvent dispersal. An SEM image of a cross-section perpendicular to the film surface (surface normal vertical) is shown in Figure 4a. The bright regions in the image correspond to the aluminosilicate phase, although the secondary electron (SE) signal is also sensitive to surface topography. The aluminosilicate layers run parallel to the surface of the film and the interlayer spacing has a range of 31 ± 5 nm, in agreement with the SAXS data ($d_l = 33.0 \pm 3.3$ nm). The SEM images also show structure

(37) Coulon, G.; Russell, T. P.; Deline, V. R.; Green, P. F. *Macromolecules* **1989**, *22*, 2581–2589.
(38) Fukunaga, K.; Elbs, H.; Magerle, R.; Krausch, G. *Macromolecules* **2000**, *33*, 947–953.
(39) Ahn, J. H.; Zin, W. C. *Macromolecules* **2000**, *33*, 641–644.
(40) Zhu, L.; Huang, P.; Chen, W. Y.; Weng, X.; Cheng, S. Z. D.; Ge, Q.; Quirk, R. P.; Senador, T.; Shaw, M. T.; Thomas, E. L.; Lotz, B.; Hsiao, B. S.; Yeh, F.; Liu, L. *Macromolecules* **2003**, *36*, 3180–3188.

Table 2. Parameters from 2-D SAXS from Compound H34 (Figure 2)

line	s_y (nm^{-1})	D_y (nm)	s_x (nm^{-1})	D_x (nm)	integrated intensity (relative)
1st layer	0.030 ± 0.003	33.0 ± 3.3	0 ± 0.005		100
2nd layer	0.059 ± 0.003	16.8 ± 0.9	0 ± 0.006		1.9 ± 0.2
outer row	−0.03 to 0.03		0.046 ± 0.004	21.7 ± 1.9	76.7 ± 0.9
inner row	0.014 ± 0.003	71 ± 14	0.025 ± 0.003	39.2 ± 4.5	11.0 ± 0.4

along each aluminosilicate layer with a mean repeat spacing of 23.6 ± 3 nm as determined by the Fourier transforms (FT) of several images. Although some of the sheets appear to have polymer (dark) channels running through them, these features along the edge of each sheet must be interpreted with caution, as the SE signal depends upon the topography of the freeze-fractured surface.

The in-plane structure of the sheets was imaged via bright-field TEM of thin sections (50 to 100 nm) cut parallel to the film surface. As shown in Figure 4b, the aluminosilicate phase (dark) formed a well-ordered 2-D hexagonal mesh with a spot spacing of 21.2 ± 1.8 nm (row spacing 18.3 ± 1.6 nm). These 2-D modulations of aluminosilicate density within each layer agree well with the strong in-plane ordering seen in the SAXS pattern (d_r = 21.7 ± 1.9 nm). These structural features were also evident in individual layers isolated by solvent-dispersal of the hybrid material.[33] As shown in the Figure 5, AFM images of individual sheets were quite flat and the average height (26.3 ± 3.0 nm) was consistent with the SAXS layer spacing (d_l = 33.0 ± 3.3 nm). Using a higher magnification and large tapping-mode amplitude, a hexagonal pattern with a row spacing of 23.5 ± 1.0 nm could just be resolved (Figure 5c).

The structure of the PEO-aluminosilicate domain within individual sheets was examined using the atomic number sensitivity of annular dark-field STEM imaging. In Figure 4c,d (aluminosilicate bright), the 2-D hexagonal pattern is readily apparent and the enrichment of silicon within the mesh framework was confirmed using parallel electron energy loss spectroscopy (PEELS). The dark regions in the hexagonal mesh could correspond to dimples in the PEO-aluminosilicate domain (Figure 1c), or "holes" where the PEO-aluminosilicate phase was completely excluded (Figure 1d). In Figure 4c, some of the spots are considerably darker than others. This variation is readily accounted for if the darker spots correspond to "holes" through the PEO-aluminosilicate and the brighter spots correspond to dimples in the PEO-aluminosilicate layer. For this model, compounds with a larger PEP volume fraction relative to PEO-aluminosilicate volume fraction should have sheets with more "holes" and fewer dimples. Supporting this prediction, TEM/STEM images show almost exclusively darker spots ("holes") for isolated sheets from compound **H28**, some brighter spots (dimples) for compound **H34**, more brighter spots for compound **H39** and the largest fraction of brighter spots for compound **H44**.

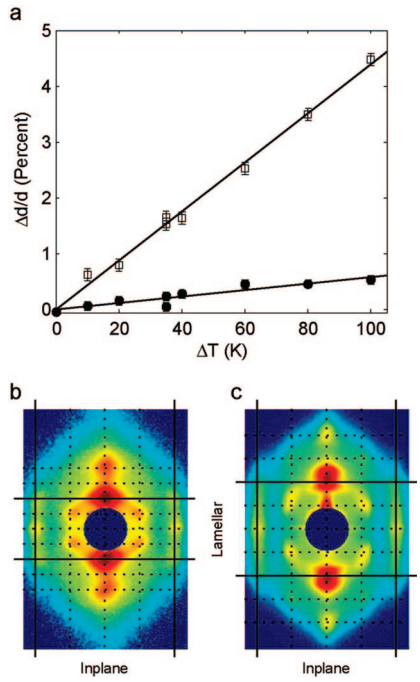

Figure 3. Hybrid material anisotropy. Percent change in lamellar (open squares) and in-plane (closed circles) repeat spacings of compound **H34** as a function of temperature (263 K to 363 K) (a). Along the lamellar direction the linear thermal expansion coefficient (4.33 ± 0.11 × 10^{-4} K^{-1}) is 7.5 ± 1 times the expansion coefficient in the in-plane direction (5.8 ± 0.8 × 10^{-5} K^{-1}). 2-D SAXS (logarithmic scale) from compound **H34** swollen by cyclohexane (d_l = 50 ± 1 nm; d_r = 21.7 ± 1.9 nm) (b) and following re-evaporation of solvent (d_l = 32.8 ± 0.5nm; d_r = 21.7 ± 1.9 nm) (c).

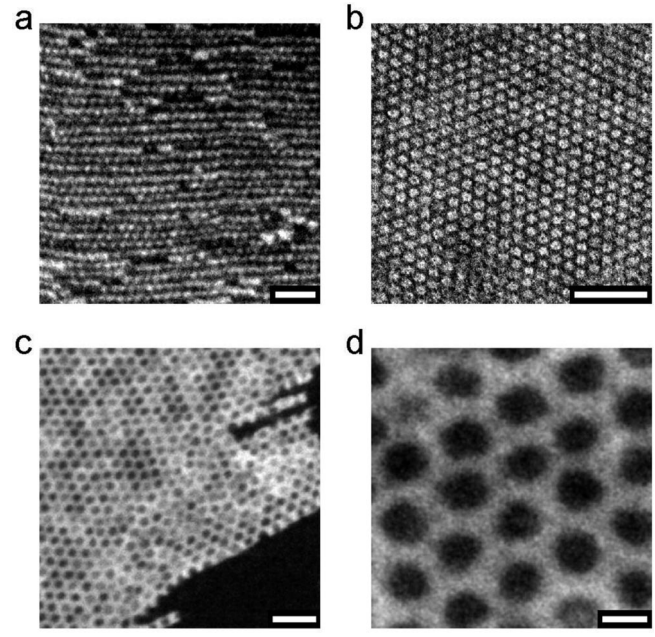

Figure 4. Electron micrographs of compound **H34**. SEM image (aluminosilicate bright) of the bulk material for a cross-section perpendicular to the surface (surface normal vertical) (a, 100 nm scale bar). Bright-field TEM (aluminosilicate dark) of a thin (~50 nm) section cut parallel to the surface (b, 100nm scale bar). Dark-field STEM image (aluminosilicate bright) of an individual sheet isolated by dispersion in solvent (c, 100 nm scale bar) and a higher magnification image of the 2-D mesh structure (d, 20 nm scale bar).

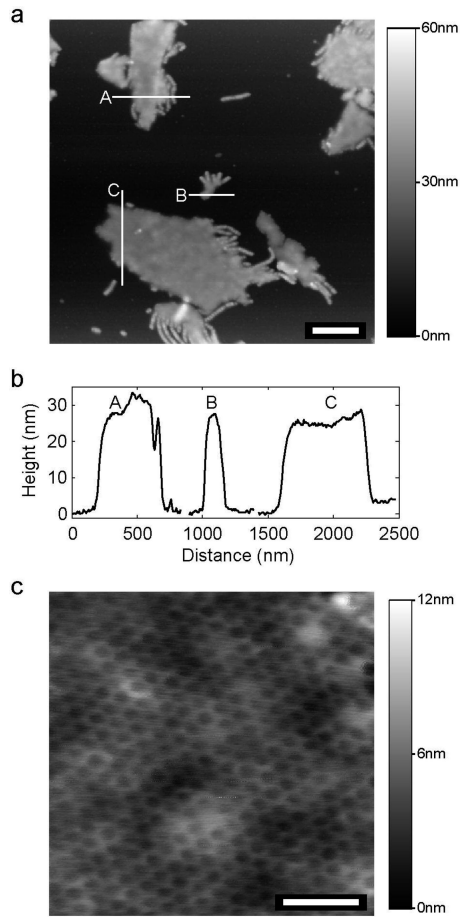

Figure 5. Tapping-mode AFM image of solvent-dispersed sheets of compound **H34** supported on a silicon substrate (a, scale bar 500nm). Sections across three sheets (A, B, C) have a mean height of 26.3 ± 3.0 nm (b). Higher magnification image of single sheet showing the hexagonal pattern (row spacing 23.5 ± 1.0 nm) observed for large amplitude tapping (c, scale bar 100 nm).

To further test the model, isolated sheets of compounds **H34** and **H44** were imaged in a field-emission SEM using both dark-field (STEM) and secondary electron (SE) signals as shown in Figure 6. Compound **H34** should have a larger fraction of "holes" than compound **H44** because it has a larger ratio of PEP to PEO-aluminosilicate volume fractions (f_{PEP}:$f_{PEO+aluminosilicate}$). Furthermore, the SE imaging mode may distinguish between "holes" and dimples as the appearance of individual dimples could differ depending on whether they are on the top or the bottom of the PEO-aluminosilicate domain. In contrast, dimples on the top or bottom of the sheet should appear the same in STEM mode because the electrons pass through the sheet and are sensitive to the integrated scattering cross section along their path.

For compound **H34**, the spots in the STEM image (Figure 6a, aluminosilicate bright) and SE image (Figure 6b) form a regular grid. Although a few spots appear brighter than average, most spots in the SE image (Figure 6b) have the same appearance, consistent with "holes" in the PEO-aluminosilicate sheet. In contrast, in the STEM image of compound **H44** (Figure 6c) only a small number of the spots are dark. Furthermore, a sizable fraction of the spots evident in the STEM image (Figure 6c) cannot be resolved in the SE image (Figure 6d). This difference in contrast is consistent with having dimples on either the top or bottom of the sheet.

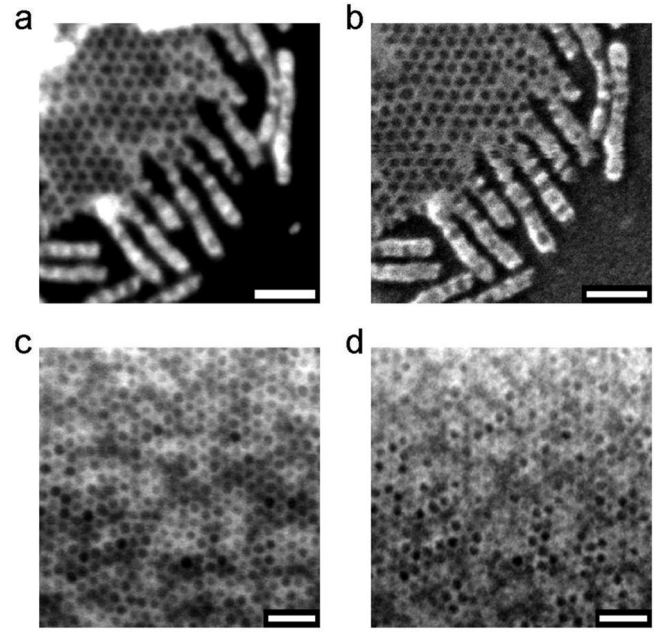

Figure 6. Solvent-dispersed sheets of compounds **H34** (a, b) and **H44** (c, d) imaged via dark-field STEM (a, c) and the secondary electron SEM signal (b, d). In all images the scale bar is 100 nm and the aluminosilicate phase is bright.

These results suggest the hexagonal pattern in the PEO-aluminosilicate domains consists of mixture of dimples and "holes".

Finally, despite the apparent hexagonal symmetry of the sheet structure, a curious feature was often seen at the edges of sheets. Frequently, as shown in Figure 7a, alternating rows of the meshwork would terminate while the remaining rows continued as individual strands. Isolated strands were also present (Figure 7b) and were more prevalent for the thinner aluminosilicate sheets of compounds **H28** and **H34** and for solutions that had been sonicated longer, suggesting the strands formed by breaking from sheets.[41] As shown in Figure 7c, the sheet structure also broke up into strands at the edges of microtomed sections. In a few of instances, alternating strands were even observed within isolated sheets as shown in Figure 7d. Thus, the sheets appear to possess a direction along which they preferentially form strands.

Internal Domain Structure. One approach to form self-assembled, hierarchical materials is through the inclusion of blocks with internal structure.[42,43] For these hybrid materials, several types of structural correlation are evident in wide-angle X-ray scattering. In Figure 8a, the outermost peak (d_{CC} = 0.48 ± 0.01 nm, s = 2.08 ± 0.04 nm^{-1}) corresponds to chain−chain correlations within the PEP and PEO blocks as well as correlations between the alkyl side chains within the PHMA block. Within the PHMA block, the difference in polarizability and flexibility between the methacrylate backbone and alkyl side chains leads to a structure where rows of aligned polymer backbones are spaced apart by their

(41) Warren, S. C.; Disalvo, F. J.; Wiesner, U. *Nat. Mater.* **2007**, *6*, 156–161.
(42) Muthukumar, M.; Ober, C. K.; Thomas, E. L. *Science* **1997**, *277*, 1225–1232.
(43) Ikkala, O.; ten Brinke, G. *Science* **2002**, *295*, 2407–2409.

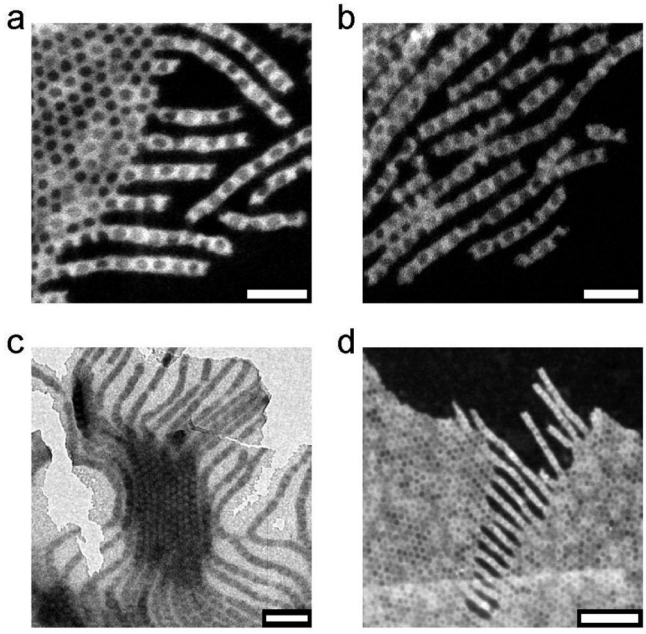

Figure 7. Dark-field STEM image of the edge of a single sheet of compound **H34** isolated by solvent dispersal shows how alternating rows terminate while the remaining rows continue as individual strands (a, aluminosilicate bright, 100 nm scale bar). Dark-field STEM image of individual strands of compound **H34** (b, aluminosilicate bright, 100 nm scale bar). Bright-field TEM of the edge of a thin (~50 nm) section of the bulk material (compound **H34**) cut parallel to the sample surface (c, aluminosilicate dark, 100 nm scale bar). Dark-field STEM image of a single sheet of compound **H44** isolated by solvent dispersal showing strand formation within the middle of a sheet (d, aluminosilicate bright, 200 nm scale bar).

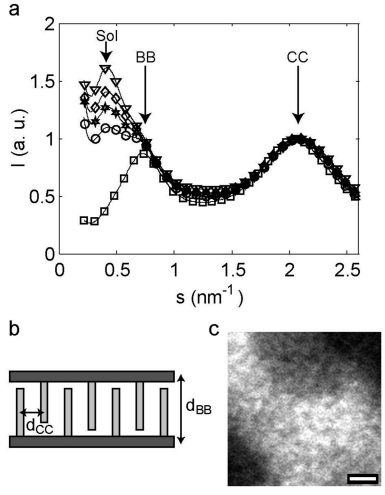

Figure 8. Wide angle X-ray scattering (WAXS) data from the parent ABC copolymer (squares), **H28** (circles), **H34** (hexagram), **H39** (diamonds), and **H44** (triangles) hybrid materials show correlations between the alkyl chains ($d_{CC} = 0.48 \pm 0.01$ nm) in all three domains, the polymer backbones within the PHMA domains ($d_{BB} = 1.38 \pm 0.03$ nm), and the aluminosilicate particles in the PEO-aluminosilicate domains ($d_{SOL} = 2.4 \pm 0.3$ nm) (a). Schematic of PHMA structure where parallel backbones (dark, horizontal) are spaced apart by their side-chains (light, vertical) (b). Dark-field TEM (aluminosilicate bright, 5nm scale bar) showing structure within the PEO-aluminosilicate domain (c).

alkyl side chains[44] as illustrated in Figure 8b. These correlations between polymer backbones within the PHMA block gives rise to the intermediate peak ($d_{BB} = 1.38 \pm 0.03$ nm, $s = 0.72 \pm 0.02$ nm^{-1}) which corresponds to that reported for WAXS from PHMA homopolymers ($d_{BB} = 1.40$ nm).[44] The innermost peak ($d_{SOL} = 2.4 \pm 0.3$ nm, $s = 0.416 \pm 0.05$ nm^{-1}) is present only in the hybrid materials and reflects correlations between the densely packed aluminosilicate particles within the PEO-aluminosilicate domain.[19,41] This structure is also apparent in high magnification dark-field STEM images (Figure 8c) of individual PEO-aluminosilicate domains.

Parent Copolymer Structure. The PEO-aluminosilicate domains in the hybrid material have a larger volume fraction and incompatibility with the PEP and PHMA blocks than the PEO domains in the parent ABC copolymer. Thus, the hybrid materials and the parent copolymer can have different morphologies. In the parent PEP-*b*-PEO-*b*-PHMA copolymer, the large volume fraction of the PHMA domain ($f_{PHMA} = 0.74 > f_{PEP} = 0.15$, $f_{PEO} = 0.11$) should favor morphologies in which the PEP and PEO blocks form micellar or cylindrical domains[10] surrounded by a matrix of PHMA. Since the mixing enthalpy of the A and C blocks is relatively small ($\chi_{PEP/PHMA}N < \chi_{PEP/PEO}N$, $\chi_{PEO/PHMA}N$), morphologies with optional PEP/PHMA domain interfaces should be favored. Earlier experimental studies of ABC copolymers in this regime have reported a number of morphologies including the "spheres-on-spheres",[45] "core-shell" cylinders,[46] "rings-at-cylinders"[46] and "helices-around-cylinders"[13] structures.

Casting from solvent did not align the parent ABC copolymer morphology so samples were aligned using reciprocating shear.[47–50] 2-D SAXS from these samples were consistent with a hexagonal structure aligned with the shear axis.

This alignment is evident in SAXS data taken with the X-ray beam directed perpendicular to the shear axis (horizontal) as shown in Figure 9a. The integrated angular intensity of the inner peak (Figure 9c) had a FWHM of ~33° concentrated perpendicular to the shear axis. In contrast, SAXS data taken with the X-ray beam parallel to the shear axis (Figure 9d,f) exhibited 6-fold symmetry, consistent with a hexagonal lattice. The individual scattering peaks were quite broad as is evident in the plots of radial averaged scattering intensity in Figure 9b,e. The bright inner ring ($s_0 = (2.63 \pm 0.05) \times 10^{-2}$ nm^{-1}) corresponded to a repeat spacing of 38.0 ± 0.7 nm while the broad second peak at $3^{1/2} \times s_0$ and shoulder at $7^{1/2} \times s_0$ are consistent with the allowed reflections for a hexagonal unit cell. Thus, morphologies in which the PEP and PEO domains form a cylindrical core are consistent with SAXS from shear-aligned samples.

(44) Beiner, M.; Kabisch, O.; Reichl, S.; Huth, H. *J. Non-Cryst. Solids* **2002**, *307*, 658–666.
(45) Breiner, U.; Krappe, U.; Jakob, T.; Abetz, V.; Stadler, R. *Polym. Bull.* **1998**, *40*, 219–226.
(46) Breiner, U.; Krappe, U.; Abetz, V.; Stadler, R. *Macromol. Chem. Phys.* **1997**, *198* (4), 1051–1083.
(47) Keller, A.; Pedemonte, E.; Willmouth, F. M. *Nature (London)* **1970**, *225*, 538–539.
(48) Kannan, R. M.; Kornfield, J. A. *Macromolecules* **1994**, *27*, 1177–1186.
(49) Leist, H.; Maring, D.; Thurn-Albrecht, T.; Wiesner, U. *J. Chem. Phys.* **1999**, *110*, 8225–8228.
(50) Stangler, S.; Abetz, V. *Rheol. Acta* **2003**, *42*, 569–577.

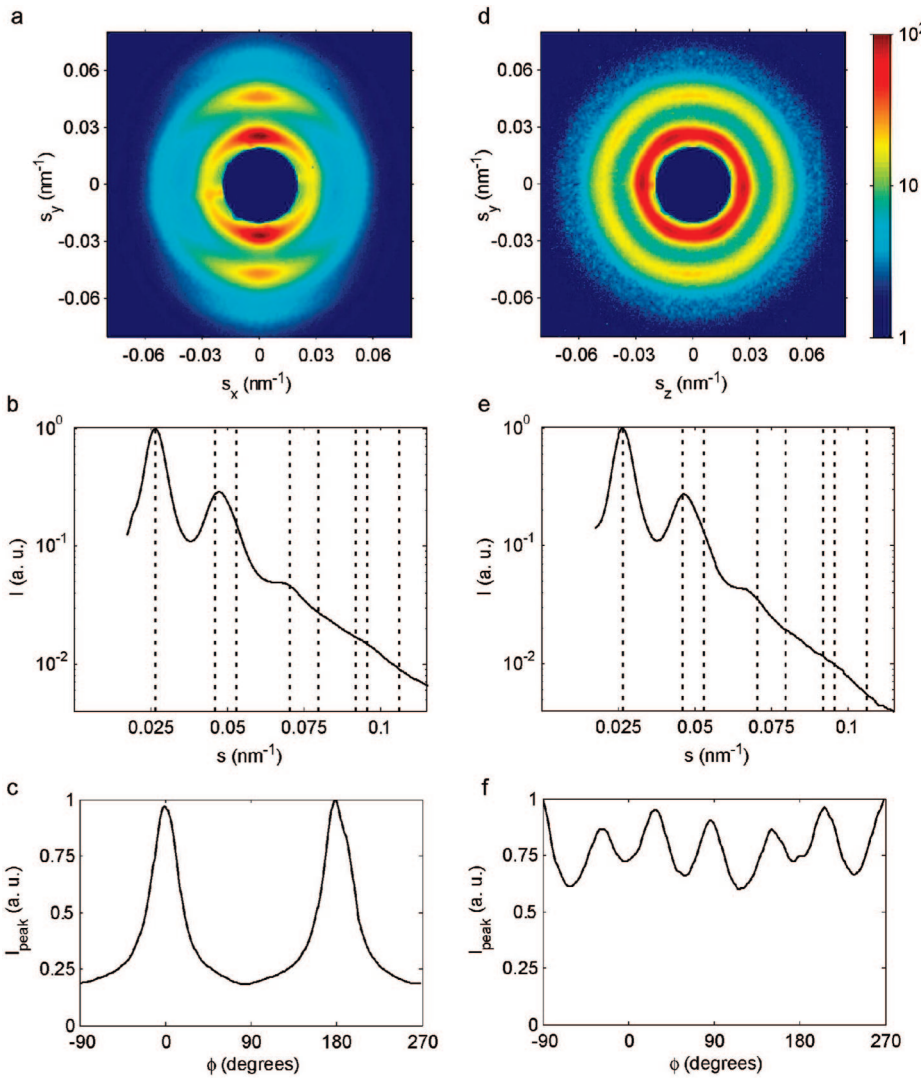

Figure 9. 2-D SAXS (logarithmic scale) from a shear-aligned specimen of the parent ABC block copolymer (a, d). The shear direction is horizontal in (a) and along the X-ray beam direction in (d), while the surface normal of the sample is vertical in both images. Radial averages (b,e) in both cases show a main peak at $s = (2.63 \pm 0.05) \times 10^{-2}$ nm^{-1} (repeat spacing of 38.0 ± 0.7 nm) and the dotted vertical lines indicate the allowed reflections for a hexagonal lattice. The angular dependence of the main peak intensity shows alignment perpendicular to the shear direction (c) with some 6-fold (f) symmetry within this plane.

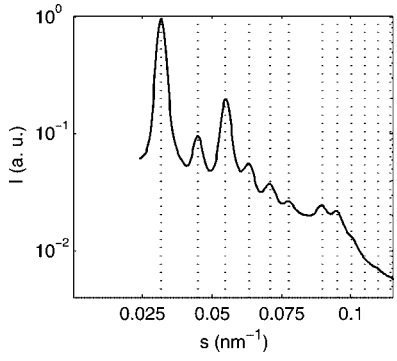

Figure 10. Powder-averaged SAXS from the parent ABC block copolymer following annealing at 100C in a saturated vapor of cyclohexane. The dotted lines correspond to a simple cubic unit cell with a lattice size of 31.1 ± 0.3 nm.

However, a different morphology formed in samples prepared by annealing in a cyclohexane atmosphere. Figure 10 shows a powder average of scattering from a solvent-annealed sample. Surprisingly, the observed scattering peaks could be indexed to a simple cubic lattice ($s_0 = 0.0322 \pm 0.0003$ nm^{-1}, repeat spacing of 31.1 ± 0.3 nm) with peaks position at relative positions of $s/s_0 = 1, 2^{1/2}, 3^{1/2}, 4^{1/2}, 5^{1/2}, 6^{1/2}, 8^{1/2}$, and $9^{1/2}$. Heating or cooling the sample changed the lattice size but not the relative position of the peaks.

After annealing at elevated temperature (200 °C), neither the cubic or hexagonal morphologies changed significantly and higher temperatures caused thermal breakdown of the polymer. However, the hexagonal morphology could be transformed into the cubic morphology by annealing at 100 °C in a cyclohexane vapor while shearing the cubic morphology at ~75 °C converted it to the hexagonal morphology. As in other block copolymer systems,[51,52] the copolymer can be kinetically trapped in distinct structures. Unfortunately, the low glass temperature of all three blocks made EM imaging of the parent polymer challenging, since the structure of thin sections is only preserved at cryogenic

(51) Ott, H.; Abetz, V.; Aldstadt, V. *Macromolecules* **2001**, *34* (7), 2121–2128.
(52) Huang, H.; Zhang, F.; Hu, Z.; Du, B.; He, T.; Lee, F. K.; Wang, Y.; Tsui, O. K. C. *Macromolecules* **2003**, *36*, 4084–4092.

temperatures and a cryo-EM stage was not available. Although SAXS from the parent ABC block copolymer is consistent with micellar or cylindrical PEP and PEO domains, further work will be required to determine the equilibrium morphology of the copolymer.

Discussion

SAXS and microscopy data from these hybrid materials show a lamellar morphology ($d_l \sim 33$ nm) in which each PEO-aluminosilicate domain is hexagonally patterned ($d_r \sim 23$ nm) with "holes" and/or dimples. The structure of the PEO-aluminosilicate domains has some similarities to the minority phase in the Hexagonally Perforated Lamellae (HPL) morphology observed in diblock copolymers.[53,54] However, the HPL morphology is believed to be metastable in diblock copolymers and is only found in a small region of the phase diagram.[54] Indeed, the HPL morphology was not observed in earlier studies of diblock PEO-b-PHMA copolymer/ aluminosilicate copolymers.[21] In contrast, the present ABC copolymer/aluminosilicate morphology forms over quite a wide range of volume fractions ($f_{PEO+aluminosilicate} = 0.28$ to at least 0.44) suggesting the small PEP block has an important influence on the morphology.

The PEP block should form distinct domains because the enthalpy for mixing with the PEO-aluminosilicate domain is truly prohibitive ($\chi_{PEP/PEO\text{-}aluminosilicate}N > \chi_{PEP/PEO}N \approx 350$) while the enthalpy for mixing with the PHMA block is also large ($\chi_{PEP/PHMA}N \approx 50$). Because the volume fraction of the PEP block is small ($f_{PEP} \sim 0.1$), round micellar PEP domains have the smallest contact area per unit volume. Within each sheet, the best packing for these micellar PEP domains is a 2-D hexagonal array (Figures 1e–f). The optimal position and shape of PEP domains depends upon a tradeoff between chain stretching and interfacial area. In the "balls-in-lamellae"[10] structure shown in Figure 1b, the burial of the PEP domain within the PEO-aluminosilicate layer incurs a large enthalpic penalty because the surface tension of the PEP/PEO-aluminosilicate interface is larger than that of a PEP/PHMA interface.

As shown in Figure 1c, moving the PEP micelle to one side of the PEO-aluminosilicate sheet reduces the area of the PEP/PEO-aluminosilicate interface at the cost of forming a PEP/PHMA interface. Alternatively, as proposed by Bailey et al.,[20] the PEP domain can form a pillar spanning the PEO-aluminosilicate domain as shown in Figure 1d. Although both structures reduce the PEP/PEO-aluminosilicate interface, the dimple structure is likely to be favored for smaller PEP micelles while the pillared structure may suit larger PEP micelles. Thus, the hexagonal structure observed within each sheet is likely to reflect the presence of an array of round PEP micelles forming dimples and pillars in the PEO-aluminosilicate domains.

These hexagonally patterned sheets are the main structural element in the hybrid materials. However, the curious strand features in Figure 7 and inner Bragg reflections in Figure 2 ($|s_x| = 0.025 \pm 0.003$ nm^{-1}, $|s_y| = 0.014 \pm 0.003$ nm^{-1}) suggest the presence of additional periodic structure. The hexagonal patterning of the sheets cannot account for these inner Bragg reflections as they have an in-plane period of 39.2 ± 4.5 nm (Table 2), approximately twice the row spacing of "holes" in the individual sheets ($d_r = 21.7 \pm 1.9$ nm). However, the inner Bragg reflections share the fiber-type alignment of the lamellar structure and their position relative to the lamellar and outer row lines is consistent with a "doubled" unit cell (height $= 2 \times d_l$, in-plane period $= 2 \times d_r$) even after changes to the lamellar lattice following heating or solvent uptake. Consequently, these reflections are likely to result from the hexagonally patterned sheet morphology itself or a structure commensurate with it.

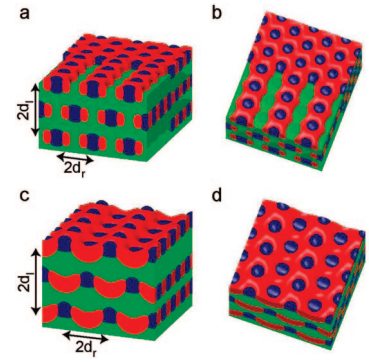

Figure 11. Structural models of unit-cell doubling. If strand formation is correlated between successive sheets (a, b) the strands form a unit cell doubled along two lattice directions (height $= 2 \times d_l$, width $= 2 \times d_r$). Alternatively, the symmetry of the unit cell can be broken by anticorrelated undulations (~2.2 nm RMS) in sheets in successive layers (c, d).

Given the individual strands observed by electron microscopy (Figure 7), one possibility is that in some parts of the sample, layers of sheets transform into alternating layers of strands (Figure 11a,b). Such a change of the PEO-aluminosilicate domains from 2-D sheets to 1-D strands could be favored in regions with a lower PEO-aluminosilicate volume fraction and then be kinetically trapped during the solvent-casting process.[19] As shown in Figures 11a and 11b, this structure naturally forms a unit cell in which both the unit cell height ($2 \times d_l$) and row spacing ($2 \times d_r$) are doubled relative to the lamellar structure shown in Figure 1f. In the strand structure shown in Figures 11a and 11b, the PEO-aluminosilicate volume fraction ($f_{PEO+aluminosilicate} = 0.28$) is assumed to be a little smaller than the lamellar structure ($f_{PEO+aluminosilicate} = 0.33$) but the exact PEO-aluminosilicate volume fraction in the strands is not known. Depending on the exact structure of strands, roughly 6% to 15% of the volume of compound **H34** would need to have this morphology to account for the intensity of the inner Bragg Reflections (Table 2).

However, the strands need not be present in the bulk material and the inner Bragg reflections could reflect broken hexagonal symmetry within the sheet structure. For example, even though every row appears identical in the EM projections, out-of-plane modulations such as

(53) Hamley, I. W.; Koppi, K. A.; Rosedale, J. H.; Bates, F. S.; Almdal, K.; Mortensen, K. *Macromolecules* **1993**, *26*, 5959–5970.
(54) Hajduk, D. A.; Takenouchi, H.; Hillmyer, M. A.; Bates, F. S.; Vigild, M. E.; Almdal, K. *Macromolecules* **1997**, *30*, 3788–3795.

those shown in Figure 11c,d cannot be excluded. Lamellar structures are unstable to undulatory modes[55,56] and the gentle undulations (2.2nm RMS amplitude) illustrated in Figure 11c,d are sufficient to account for the intensity of the inner Bragg Reflections (Table 2). Although it seems more probable that there are alternating layers of strands within the bulk material, further study will be required to understand whether the strands are predominantly a structural intermediate formed during solvent casting or a product of the solvent isolation procedure.[41]

Conclusion

A PEP-*b*-PEO-*b*-PHMA triblock copolymer (volume fractions $f_{PEP} = 0.15$, $f_{PEO} = 0.11$, $f_{PHMA} = 0.74$) was used as a structure-directing agent to form self-assembled block copolymer/aluminosilicate nanocomposites in which the PEP volume fraction ($0.09 \leq f_{PEP} \leq 0.12$) was much smaller than that of the PEO-aluminosilicate ($0.28 \leq f_{PEO+Aluminosilicate} \leq 0.44$) and PHMA ($0.47 \leq f_{PHMA} \leq 0.60$) domains. The volume fractions of the parent copolymer and hybrid materials were quite different, and SAXS data indicated that the structure of the hybrid materials was indeed quite different from that of solvent-cast and shear-aligned samples of the parent ABC copolymer. For the hybrid materials, X-ray scattering and electron microscopy data indicate that the PEO-aluminosilicate phase formed hexagonally patterned layers aligned parallel to the surface of the film (lamellar repeat spacing = 33.0 ± 3.3 nm, in-plane row spacing = 21.7 ± 1.9 nm). Level set modeling confirmed that this patterning of the PEO-aluminosilicate sheets is consistent with micellar PEP domains forming either pillars through the sheet, as in the proposed "pillared-lamellae" structure,[20] or dimples at the surface of the sheet. Finally, WAXS confirmed the hybrid materials possess structure within the PHMA and PEO-aluminosilicate domains at the 1−3 nm length-scale. These results establish that ABC triblock copolymers can be used to direct the assembly of inorganic precursors into hybrid materials with complex, hierarchical structures.

Acknowledgment. We thank Scott Warren and Marleen Kamperman for help with synthesis and characterization of polymers and Marty Novak for expert machining. This work was supported by the National Science Foundation (DMR-0605856, DMR-0404195, DMR-0225180, and DMR-0079992) and by Department of Energy BER Grant DE-FG02-97ER62443.

CM702842B

(55) Rosedale, J. H.; Bates, F. S.; Almdal, K.; Mortensen, K.; Wignall, G. D. *Macromolecules* **1995**, *28*, 1429–1443.

(56) Cohen, Y.; Brinkmann, T.; Thomas, E. L. *J. Chem. Phys.* **2001**, *114*, 984–992.